

RKDG methods with multi-resolution WENO limiters for solving steady-state problems on triangular meshes

Jun Zhu¹, Chi-Wang Shu² and Jianxian Qiu³

Abstract

In this paper, we design high-order Runge-Kutta discontinuous Galerkin (RKDG) methods with multi-resolution weighted essentially non-oscillatory (multi-resolution WENO) limiters to compute compressible steady-state problems on triangular meshes. A new troubled cell indicator is constructed to identify triangular cells in which the application of the limiting procedures is required. In such troubled cells, the multi-resolution WENO limiting methods are used to the hierarchical L^2 projection polynomial sequence of the DG solution. Through using the RKDG methods with multi-resolution WENO limiters, optimal high-order accuracy can be gradually reduced to first order in the triangular troubled cells, so that the shock wave oscillations can be well suppressed. In steady-state simulations on triangular meshes, the numerical residual converges to near machine zero. The proposed spatial reconstruction methods enhance the robustness of classical DG methods on triangular meshes. The good results of these RKDG methods with multi-resolution WENO limiters are verified by a series of two-dimensional steady-state problems.

Key Words: RKDG method, steady-state problem, multi-resolution WENO limiter, triangular mesh, machine zero.

AMS(MOS) subject classification: 65M60, 35L65

¹State Key Laboratory of Mechanics and Control of Mechanical Structures. Key Laboratory of Mathematical Modelling and High Performance Computing of Air Vehicles (NUAA), MIIT. Nanjing University of Aeronautics and Astronautics, Nanjing, Jiangsu 210016, P.R. China. E-mail: zhujun@nuaa.edu.cn. Research is supported by NSFC grant 11872210 and Grant No. MCMS-I-0120G01.

²Division of Applied Mathematics, Brown University, Providence, RI 02912, USA. E-mail: chiwang_shu@brown.edu. Research is supported by AFOSR grant FA9550-20-1-0055 and NSF grant DMS-2010107.

³School of Mathematical Sciences and Fujian Provincial Key Laboratory of Mathematical Modeling and High-Performance Scientific Computing, Xiamen University, Xiamen, Fujian 361005, P.R. China. E-mail: jxqiu@xmu.edu.cn. Research is supported by NSFC grant 12071392.

1 Introduction

In this paper, we design high-order Runge-Kutta discontinuous Galerkin (RKDG) methods [8, 9, 10, 12] with multi-resolution WENO limiters [51] to compute two-dimensional steady-state Euler equations

$$\begin{cases} f(u)_x + g(u)_y = 0, \\ u(x, y) = u_0(x, y), \end{cases} \quad (1.1)$$

on triangular meshes. This is a method to compute (1.1) by solving two-dimensional unsteady Euler equations

$$\begin{cases} u_t + f(u)_x + g(u)_y = 0, \\ u(x, y, 0) = u_0(x, y). \end{cases} \quad (1.2)$$

We use high-order DG methods for spatial discretization and the explicit and nonlinearly stable Runge-Kutta methods [40, 13] for temporal discretization to make the numerical residuals converge to near machine zero. The main work is to construct a new troubled cell indicator to identify triangular cells in which the application of the higher-order limiting procedures is required, and then use the DG methods with the multi-resolution WENO limiters [51] to compute two-dimensional steady-state problems on triangular meshes. The new troubled cell indicator is needed to obtain steady state convergence to near machine zero.

When the numerical residual of the two-dimensional unsteady Euler equations (1.2) is near machine zero, the numerical solution of two-dimensional steady-state Euler equations (1.1) is achieved. There will be strong discontinuities when solving (1.1) and (1.2). In the past, many high-resolution numerical schemes have been proposed, mainly using artificial viscosities [22, 23] or nonlinear limiters [19, 22, 42] to suppress the oscillations. Jameson et al. [21, 24] designed a third-order finite volume method with dissipation terms to simulate steady-state problems. But to accurately simulate strong shocks in the numerical simulation, they often needed to adjust some parameters in the artificial viscosity. In 1983, Harten [19] found that numerical schemes with limiters were very effective in simulating supersonic flow problems. However, when the total variation diminishing (TVD) limiters [34] were used,

it was difficult for the numerical residuals to converge to near machine zero. In 1985, Yee et al. [45] proposed the implicit TVD schemes for the steady-state calculation. Two years later, Yee et al. [44] proposed an implicit TVD scheme for hyperbolic conservation laws in curvilinear coordinates. The researchers found that the numerical residuals could not be reduced to machine zero when the classical WENO scheme [25] was used to compute the steady-state problems. In 2004, Serna and Marquina [37] designed a fifth-order accurate weighted power ENO method, which significantly improved the convergence of the numerical scheme. Three years later, Zhang and Shu [49] proposed a new WENO scheme smoothness indicator and analyzed its influence on the convergence to the steady-state solution. In 2011, Zhang et al. [48] proposed the WENO scheme to improve the convergence of the steady-state solutions of Euler equations. This new method had a good effect. But for several two-dimensional steady-state problems [48], there was still the phenomenon that the numerical residuals could not converge to machine zero. Wu et al. [43] designed a fixed-point sweeping WENO methods to compute the steady-state hyperbolic conservation laws and discussed its convergence. It was found that the numerical residuals were difficult to approach machine zero for some examples.

At present, researchers have proposed many discontinuous Galerkin (DG) methods to compute the unsteady and steady-state problems. As early as 1973, Reed et al. [36] innovatively proposed the first DG method in the study of neutron transport equations. The hybrid DG/FV methods [15, 16, 31, 46, 47] were designed for various problems. The application of a nonlinear limiter in the higher-order RKDG methods can effectively solve the problem of pseudo oscillation. Cockburn et al. [8, 9, 10, 11, 12] performed extensive research on the DG methods and applied the *minmod* type total variation bounded (TVB) limiters. Now many kinds of limiters have been developed, which are mainly divided into two categories: the slope-type limiters [2, 3, 5, 8, 9, 10, 12, 42] and the WENO limiters [1, 17, 18, 20, 25, 28, 29, 30, 32, 33]. The former can effectively solve the problem of pseudo oscillation, but the precision will decrease. When solving steady-state problems, both types

have difficulties in the RKDG methods. Especially, when solving two-dimensional steady-state Euler equations on triangular meshes, the numerical residuals often can not converge to near machine zero.

It is found that when the third-order TVD Runge Kutta method [40] and the classical finite difference WENO scheme [25, 39] are applied to simulate the steady-state problems, there is a problem that the numerical residual can not reduce to near machine zero. With further research, the scholars found that the new high-order WENO schemes [50] had good performance. These methods can have the numerical residuals to converge close to machine zero, and there is no pseudo oscillations on structured or unstructured meshes. These new multi-resolution WENO schemes have a series of spatial templates with different sizes, which make the high-order accuracy schemes gradually reduce to first-order accuracy near strong discontinuities. In this paper, the high-order RKDG methods with multi-resolution WENO limiters [51] are proposed for the first time to compute the steady-state problem on triangular meshes.

The rest parts of this paper are as follows. Section 2 introduces the RKDG methods to compute (1.2) on triangular meshes. For simulating two-dimensional steady-state problems on triangular meshes, a new troubled cell indicator and high-order limiters are designed in Section 3. In Section 4, several steady-state problems are simulated to testify the effectiveness of the designed methods. The conclusions are described in Section 5.

2 RKDG method on triangular meshes

Now we introduce the RKDG methods to compute (1.2) on triangular meshes. The DG methods have the numerical solutions on triangle cells Δ_0 . The test function space is $V_h^k = \{v(x, y) : v(x, y)|_{\Delta_0} \in \mathbb{P}^k(\Delta_0)\}$, where $\mathbb{P}^k(\Delta_0)$ represents the set of polynomials with **total degree** at most k on Δ_0 . We select the function $u_h \in V_h^k$, so that

$$\int_{\Delta_0} (u_h)_t v \, dx \, dy = \int_{\Delta_0} (f(u_h)v_x + g(u_h)v_y) \, dx \, dy - \int_{\partial\Delta_0} (f(u^h), g(u^h)) \cdot \vec{n} v \, ds, \quad (2.1)$$

for all test functions $v \in V_h^k$. The outward unit normal of the triangle boundary $\partial\Delta_0$ is $\vec{n} = (n_x, n_y)^T$. $(f(u^h), g(u^h)) \cdot \vec{n}$ is an accurate or approximate Riemann solver in the system case, and is a monotone numerical flux in the scalar case. The third-order Runge-Kutta method [41]

$$\begin{cases} u^{(1)} &= u^n + \Delta t L(u^n), \\ u^{(2)} &= \frac{3}{4}u^n + \frac{1}{4}u^{(1)} + \frac{1}{4}\Delta t L(u^{(1)}), \\ u^{n+1} &= \frac{1}{3}u^n + \frac{2}{3}u^{(2)} + \frac{2}{3}\Delta t L(u^{(2)}), \end{cases} \quad (2.2)$$

is used to design a fully discrete scheme.

3 Multi-resolution WENO limiter

This section briefly describes the construction process of a new troubled cell indicator and high-order multi-resolution WENO limiters [51] on triangular meshes.

3.1 Troubled cell indicator on triangular meshes

The objective is to identify the troubled cells on triangular meshes. If the number of troubled cells is too large, the computational cost will increase. But if the number is too small, the pseudo oscillation will occur. There have been a lot of discussions on the indicators of different troubled cells [35]. **The troubled cell indicator in this paper is a generalization of the one in [52] to triangular meshes.** Referring to Figure 3.1, Δ_ℓ , $\ell = 1, 2, 3$ represent the adjacent triangular cells of Δ_0 . $u_h(x, y, t)$ is the numerical solution of the indicator variable. If it satisfies

$$\frac{\max_{\ell=1,2,3} \left(\left| \frac{1}{|\Delta_0|} \int_{\Delta_0} u_h(x, y, t) |_{\Delta_0} dx dy - \frac{1}{|\Delta_\ell|} \int_{\Delta_\ell} u_h(x, y, t) |_{\Delta_\ell} dx dy \right| \right)}{h_0 \min_{\ell=0,1,2,3} \left(\left| \frac{1}{|\Delta_\ell|} \int_{\Delta_\ell} u_h(x, y, t) |_{\Delta_\ell} dx dy \right| \right)} \geq 1, \quad (3.1)$$

then Δ_0 is considered to be a troubled cell. Here h_0 represents the radius of the inscribed circle of Δ_0 . We will demonstrate later that this new troubled cell indicator is very effective in the calculation of steady-state problems on triangular meshes.

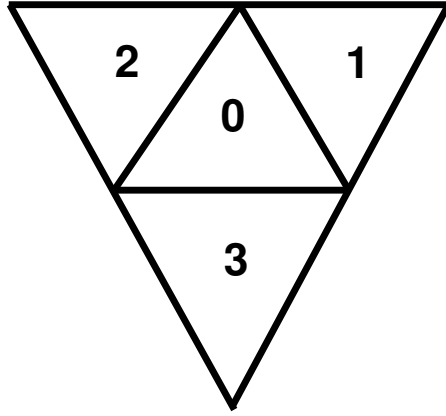


Figure 3.1: Triangular cells Δ_0 , Δ_1 , Δ_2 , and Δ_3 .

3.2 Multi-resolution WENO limiter

From now on $u_h(x, y, t)$ is written as $u_h(x, y)$ for convenience, if it does not cause confusion. Let Δ_0 be the troubled cell determined by the new troubled cell indicator. The construction process of multi-resolution WENO limiters [51] for the scalar case is briefly described in the following: We construct multiple polynomials of various degrees on Δ_0 . We adopt a local orthogonal basis over Δ_0 : $\{v_l^{(0)}(x, y), l = 0, \dots, K; K = (k+1)(k+2)/2 - 1\}$:

$$\begin{aligned}
 v_0^{(0)}(x, y) &= 1, \\
 v_1^{(0)}(x, y) &= \frac{x - x_0}{\sqrt{|\Delta_0|}}, \\
 v_2^{(0)}(x, y) &= a_{21} \frac{x - x_0}{\sqrt{|\Delta_0|}} + a_{22} \frac{y - y_0}{\sqrt{|\Delta_0|}} + a_{23}, \\
 &\dots
 \end{aligned}$$

where (x_0, y_0) and $|\Delta_0|$ are the barycenter and the area of Δ_0 , respectively. Then we solve a linear system to obtain the values of $a_{\ell m}$ by the orthogonality property:

$$\frac{1}{\int_{\Delta_0} (v_i^{(0)}(x, y))^2 dx dy} \int_{\Delta_0} v_i^{(0)}(x, y) v_j^{(0)}(x, y) dx dy = \delta_{ij}. \quad (3.2)$$

We design $q_\ell(x, y)$, $\ell = 0, \dots, k$, which satisfy

$$\int_{\Delta_0} q_\ell(x, y) v_l^{(0)}(x, y) dx dy = \int_{\Delta_0} u_h(x, y) v_l^{(0)}(x, y) dx dy, \quad l = 0, \dots, \frac{(\ell+1)(\ell+2)}{2} - 1. \quad (3.3)$$

Then we set $p_{0,1}(x, y) = q_0(x, y)$. According to [6, 26, 27], we get the polynomials

$$p_{\ell,\ell}(x, y) = \frac{1}{\gamma_{\ell,\ell}} q_\ell(x, y) - \frac{\gamma_{\ell-1,\ell}}{\gamma_{\ell,\ell}} p_{\ell-1,\ell}(x, y), \quad \ell = 1, \dots, k, \quad (3.4)$$

with $\gamma_{\ell-1,\ell} + \gamma_{\ell,\ell} = 1$ and $\gamma_{\ell,\ell} \neq 0$, together with the polynomials

$$p_{\ell,\ell+1}(x, y) = \omega_{\ell,\ell} p_{\ell,\ell}(x, y) + \omega_{\ell-1,\ell} p_{\ell-1,\ell}(x, y), \quad \ell = 1, \dots, k-1, \quad (3.5)$$

with $\omega_{\ell-1,\ell} + \omega_{\ell,\ell} = 1$. Here, $\gamma_{\ell-1,\ell}$ and $\gamma_{\ell,\ell}$ represent the linear weights, and $\omega_{\ell-1,\ell}$ and $\omega_{\ell,\ell}$ represent the nonlinear weights. We compute the smoothness indicators β_{ℓ,ℓ_2} . The smoothness indicators [25, 39] are constructed as

$$\beta_{\ell,\ell_2} = \sum_{|\alpha|=1}^{\kappa} \int_{\Delta_0} \Delta_0^{|\alpha|-1} \left(\frac{\partial^{|\alpha|}}{\partial x^{\alpha_1} \partial y^{\alpha_2}} p_{\ell,\ell_2}(x, y) \right)^2 dx dy, \quad \ell = \ell_2 - 1, \ell_2; \quad \ell_2 = 1, 2, 3, \quad (3.6)$$

where $\kappa = \ell$, $\alpha = (\alpha_1, \alpha_2)$, and $|\alpha| = \alpha_1 + \alpha_2$. Here $\beta_{0,1}$ is constructed as specified in [51].

Following [4, 7], we define

$$\tau_{\ell_2} = (\beta_{\ell_2,\ell_2} - \beta_{\ell_2-1,\ell_2})^2, \quad \ell_2 = 1, 2, 3. \quad (3.7)$$

The nonlinear weights are

$$\omega_{\ell_1,\ell_2} = \frac{\bar{\omega}_{\ell_1,\ell_2}}{\sum_{\ell=1}^{\ell_2} \bar{\omega}_{\ell,\ell_2}}, \quad \bar{\omega}_{\ell_1,\ell_2} = \gamma_{\ell_1,\ell_2} \left(1 + \frac{\tau_{\ell_2}}{\varepsilon + \beta_{\ell_1,\ell_2}} \right), \quad \ell_1 = \ell_2 - 1, \ell_2; \quad \ell_2 = 1, 2, 3. \quad (3.8)$$

Here ε is set as 10^{-6} . The final new polynomial is

$$p^{new}(x, y) = \sum_{\ell=\ell_2-1}^{\ell_2} \omega_{\ell,\ell_2} p_{\ell,\ell_2}(x, y), \quad \ell_2 = 1, 2, 3, \quad (3.9)$$

for the second-order, third-order, and fourth-order approximations, respectively.

Then we write (1.2) as

$$u_t + f(u)_x + g(u)_y = \frac{\partial}{\partial t} \begin{pmatrix} \rho \\ \rho\mu \\ \rho\nu \\ E \end{pmatrix} + \frac{\partial}{\partial x} \begin{pmatrix} \rho\mu \\ \rho\mu^2 + p \\ \rho\mu\nu \\ \mu(E + p) \end{pmatrix} + \frac{\partial}{\partial y} \begin{pmatrix} \rho\nu \\ \rho\mu\nu \\ \rho\nu^2 + p \\ \nu(E + p) \end{pmatrix} = 0. \quad (3.10)$$

Here ρ is the density, μ and ν are the velocities in x -direction and y -direction, respectively, E is the total energy, $\gamma = 1.4$, and $p = \frac{E}{\gamma-1} - \frac{1}{2}\rho(\mu^2 + \nu^2)$ is the pressure. Let the Jacobian

be $(f'(u), g'(u)) \cdot \vec{n}_i = f'(u)n_{ix} + g'(u)n_{iy}$, where $\vec{n}_i = (n_{ix}, n_{iy})^T$, $i = 1, 2, 3$, are the outward unit normals of the edges of the target cell. The eigenvectors of the Jacobian matrix [53] are

$$L_i = \begin{pmatrix} \frac{B_2 + (\mu n_{ix} + \nu n_{iy})/c}{2} & -\frac{B_1\mu + n_{ix}/c}{2} & -\frac{B_1\nu + n_{iy}/c}{2} & \frac{B_1}{2} \\ n_{iy}\mu - n_{ix}\nu & -n_{iy} & n_{ix} & 0 \\ 1 - B_2 & B_1\mu & B_1\nu & -B_1 \\ \frac{B_2 - (\mu n_{ix} + \nu n_{iy})/c}{2} & -\frac{B_1\mu - n_{ix}/c}{2} & -\frac{B_1\nu - n_{iy}/c}{2} & \frac{B_1}{2} \end{pmatrix}, \quad (3.11)$$

and

$$R_i = \begin{pmatrix} 1 & 0 & 1 & 1 \\ \mu - cn_{ix} & -n_{iy} & \mu & \mu + cn_{ix} \\ \nu - cn_{iy} & n_{ix} & \nu & \nu + cn_{iy} \\ H - c(\mu n_{ix} + \nu n_{iy}) & -n_{iy}\mu + n_{ix}\nu & \frac{\mu^2 + \nu^2}{2} & H + c(\mu n_{ix} + \nu n_{iy}) \end{pmatrix}, \quad i = 1, 2, 3, \quad (3.12)$$

and $B_1 = \frac{\gamma-1}{c^2}$, $B_2 = \frac{B_1(\mu^2 + \nu^2)}{2}$, $c = \sqrt{\gamma p/\rho}$, and $H = \frac{E+p}{\rho}$. For the relevant polynomial vectors p_0 , p_1 , p_2 , and p_3 on the troubled cell Δ_0 , the construction process of the multi-resolution WENO limiters [51] for the system case is briefly described in the following: We firstly construct the new polynomial vectors p_i^{new} , $i = 1, 2, 3$, in each \vec{n}_i -direction of the normal directions of $\partial\Delta_0$ by applying the multi-resolution WENO limiting and relevant Jacobian $f'(u)n_{ix} + g'(u)n_{iy}$, $i = 1, 2, 3$. Then we project p_0 , p_1 , p_2 , and p_3 into $\tilde{\tilde{p}}_i = L_i \cdot p_i$, $i = 1, 2, 3$, $l = 0, 1, 2, 3$. $\tilde{\tilde{p}}_i$ is a 4-component vector, and every constituent is a polynomial to the degree k . For every constituent of $\tilde{\tilde{p}}_i$, we execute the scalar case of the multi-resolution WENO limiting procedure and get the 4-component vectors on Δ_0 as \tilde{p}_i^{new} , $i = 1, 2, 3$, respectively. Then we project \tilde{p}_i^{new} into the physical space $p_i^{new} = R_i \cdot \tilde{p}_i^{new}$, $i = 1, 2, 3$. Finally, the ultimate 4-component vector on Δ_0 is

$$p^{new} = \frac{\sum_{i=1}^3 p_i^{new} |\Delta_i|}{\sum_{i=1}^3 |\Delta_i|}. \quad (3.13)$$

4 Numerical results

Now, several steady-state problems are applied to testify the effectiveness of the second-order, third-order, and fourth-order RKDG methods with multi-resolution WENO limiters (termed as the RKDG2-MRWENO, RKDG3-MRWENO, and RKDG4-MRWENO methods, respectively) on triangular meshes. For the two two-dimensional accuracy examples, the refinement is performed by a structured refinement and all triangular cells are noted as the troubled cells, in order to verify that accuracy as well as steady state convergence are not affected even if the limiter is over-used in all cells. For the other examples, (3.1) is used to detect the troubled cells. For the RKDG2-MRWENO, RKDG3-MRWENO, and RKDG4-MRWENO methods, the CFL numbers are 0.3, 0.18, and 0.1, respectively. **The numerical residual is given by**

$$\text{Res}_A = \sum_{i=1}^N \frac{|\text{R1}_i| + |\text{R2}_i| + |\text{R3}_i| + |\text{R4}_i|}{4 \times N}, \quad (4.1)$$

in which $\text{R1}_i = \frac{\partial \rho}{\partial t}|_i \approx \frac{\rho_i^{n+1} - \rho_i^n}{\Delta t}$, $\text{R2}_i = \frac{\partial(\rho\mu)}{\partial t}|_i \approx \frac{(\rho\mu)_i^{n+1} - (\rho\mu)_i^n}{\Delta t}$, $\text{R3}_i = \frac{\partial(\rho\nu)}{\partial t}|_i \approx \frac{(\rho\nu)_i^{n+1} - (\rho\nu)_i^n}{\Delta t}$, $\text{R4}_i = \frac{\partial E}{\partial t}|_i \approx \frac{E_i^{n+1} - E_i^n}{\Delta t}$. N is the total number of all triangular cells inside the computational field. The linear weights are set as $\gamma_{\ell-1,\ell} = 0.01$ and $\gamma_{\ell,\ell} = 0.99$, $\ell = 1, 2, 3$, respectively.

Example 4.1. We compute two-dimensional Euler equations (3.10). The calculation range is $(x, y) \in [0, 2] \times [0, 2]$. $\rho(x, y, \infty) = 1 + 0.2 \sin(x - y)$, $\mu(x, y, \infty) = 1$, $\nu(x, y, \infty) = 1$, and $p(x, y, \infty) = 1$ are exact steady-state solutions. Figure 4.1 shows a sample mesh. The numerical residual is demonstrated in Figure 4.2, in which the numerical residual is reduced to the minimum value of machine zero. The numerical errors and orders for the density at steady state are shown in Table 4.1. It is seen that the RKDG2-MRWENO, RKDG3-MRWENO, and RKDG4-MRWENO methods are performing well for this steady-state test case: the numerical residual settles to near machine zero, and the designed order of accuracy is achieved.

Example 4.2. The shock reflection problem. The calculation range is $(x, y) \in [0, 4] \times [0, 1]$.

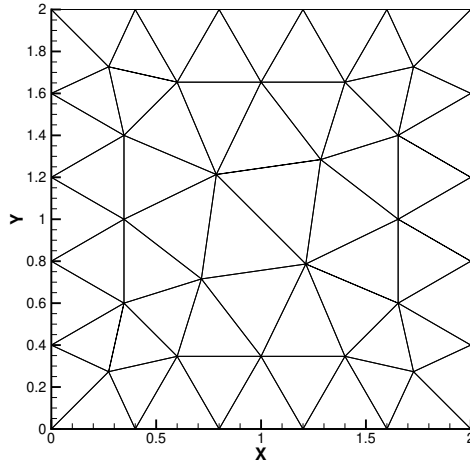


Figure 4.1: 2D Euler equations for steady-state problem. Sample mesh.

Table 4.1: 2D Euler equations for steady-state problem. Case (1). L^1 and L^∞ errors for density.

RKDG2-MRWENO method				
h	L^1 error	order	L^∞ error	order
$\frac{2}{5}$	9.20E-4		4.08E-3	
$\frac{2}{10}$	2.14E-4	2.10	1.05E-3	1.96
$\frac{2}{20}$	4.91E-5	2.13	2.44E-4	2.10
$\frac{2}{40}$	1.19E-5	2.05	6.33E-5	1.95
$\frac{2}{80}$	2.93E-6	2.02	1.61E-5	1.97
RKDG3-MRWENO method				
h	L^1 error	order	L^∞ error	order
$\frac{2}{5}$	1.77E-4		7.24E-4	
$\frac{2}{10}$	2.16E-5	3.03	1.19E-4	2.60
$\frac{2}{20}$	2.86E-6	2.92	1.68E-5	2.83
$\frac{2}{40}$	3.79E-7	2.92	2.26E-6	2.89
$\frac{2}{80}$	4.93E-8	2.94	2.92E-7	2.96
RKDG4-MRWENO method				
h	L^1 error	order	L^∞ error	order
$\frac{2}{5}$	1.91E-6		6.43E-6	
$\frac{2}{10}$	1.13E-7	4.08	5.17E-7	3.64
$\frac{2}{20}$	5.73E-9	4.30	3.34E-8	3.95
$\frac{2}{40}$	3.16E-10	4.18	2.33E-9	3.84
$\frac{2}{80}$	1.99E-11	3.99	1.33E-10	4.13

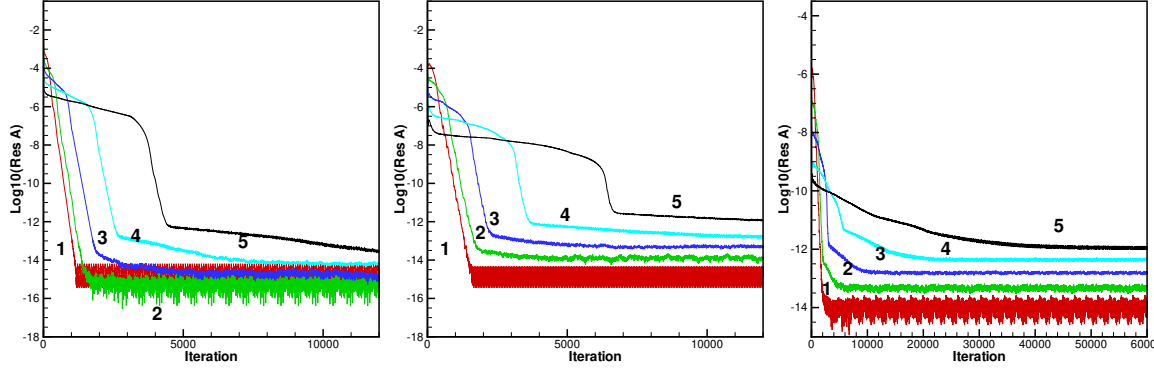


Figure 4.2: 2D Euler equations for steady-state problem. Case (1). Left: RKDG2-MRWENO method; middle: RKDG3-MRWENO method; right: RKDG4-MRWENO method. Diverse numbers represent different mesh levels of boundary points uniformly distributed from $\frac{2}{5}$ to $\frac{2}{80}$.

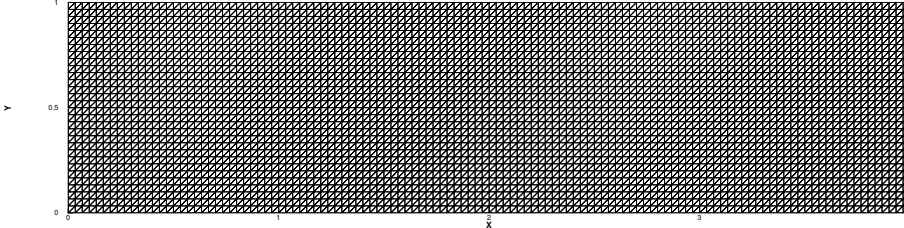


Figure 4.3: The shock reflection problem. Sample mesh.

The Dirichlet conditions are applied on the other two sides

$$(\rho, \mu, \nu, p)^T = \begin{cases} (1.0, 2.9, 0, 1.0/1.4)^T|_{(0,y,t)^T}, \\ (1.69997, 2.61934, -0.50632, 1.52819)^T|_{(x,1,t)^T}. \end{cases} \quad (4.2)$$

Figure 4.3 shows a sample mesh. Figure 4.4 shows the density contours of 15 equidistant contours from 1.14 to 2.60. Figure 4.5 shows the troubled cells identified in the termination time. It is observed that the RKDG4-MRWENO method has better resolution than that of the RKDG2-MRWENO method and RKDG3-MRWENO method, especially for the accurate capture of strong shocks. The numerical residual is shown in Figure 4.6. It is found that the average residual of the RKDG-MRWENO methods can reduce to about 10^{-12} , near machine zero.

Example 4.3. Two transonic steady-state problems of NACA0012 airfoil [38] with $M_\infty = 0.8$, $\alpha = 1.25^\circ$ and $M_\infty = 0.85$, $\alpha = 1^\circ$. The calculation range is $[-15, 15] \times [-15, 15]$. Figure

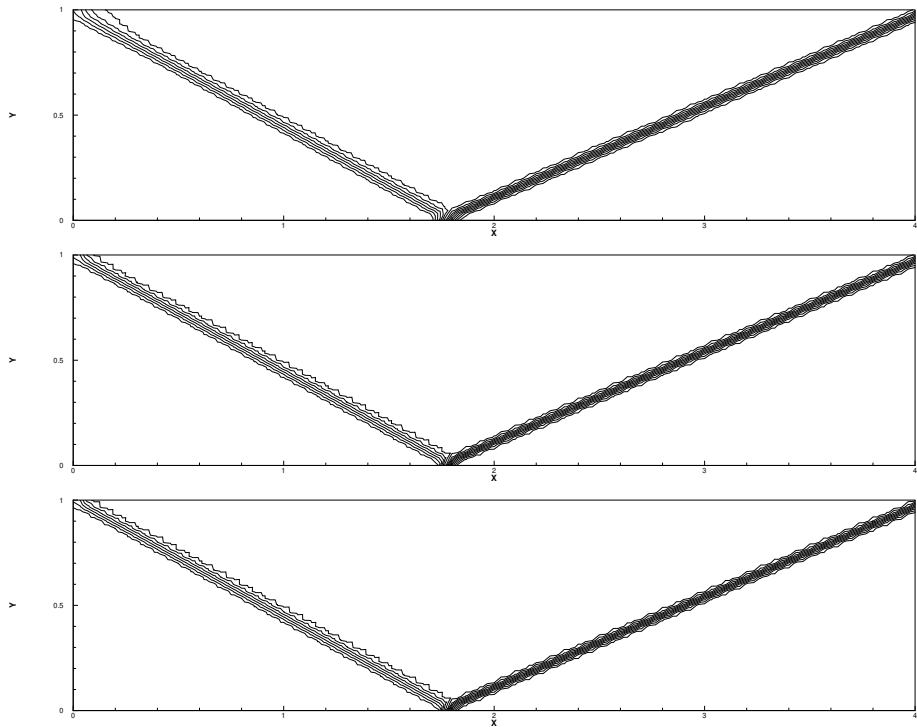


Figure 4.4: The shock reflection problem. 15 equally spaced density contours from 1.14 to 2.60. Top: RKDG2-MRWENO method; middle: RKDG3-MRWENO method; bottom: RKDG4-MRWENO method. Boundary points are $h = \frac{1}{30}$.

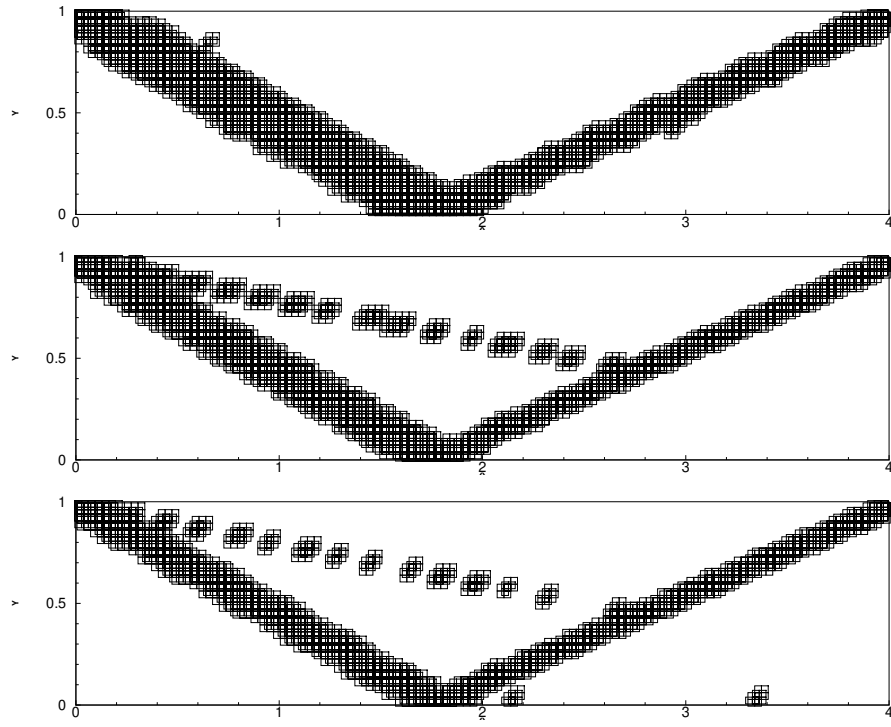


Figure 4.5: The shock reflection problem. The square represents the cells identified as troubled cells at the end of time. Top: RKDG2-MRWENO method; middle: RKDG3-MRWENO method; bottom: RKDG4-MRWENO method. Boundary points are $h = \frac{1}{30}$.

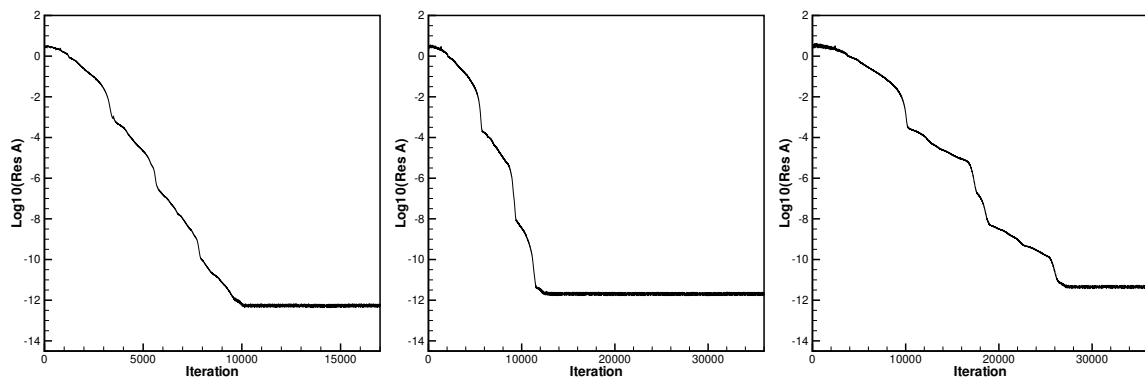


Figure 4.6: The shock reflection problem. Left: RKDG2-MRWENO method; middle: RKDG3-MRWENO method; right: RKDG4-MRWENO method. Boundary points are $h = \frac{1}{30}$.

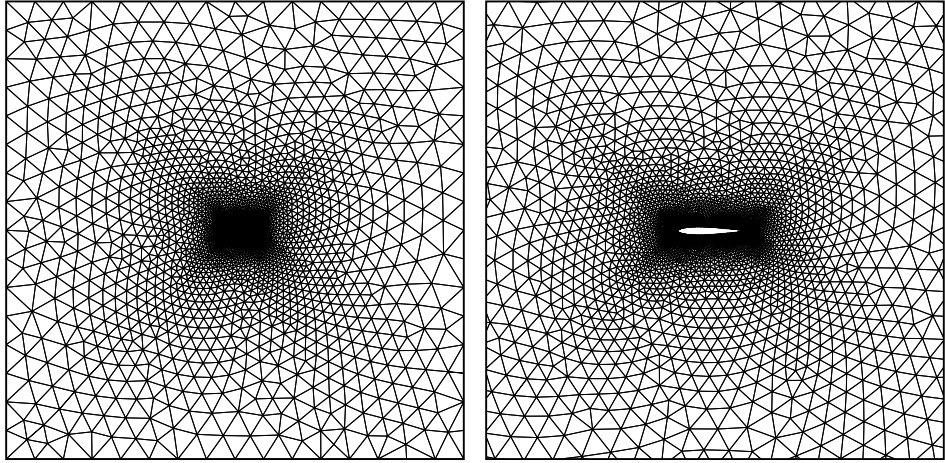


Figure 4.7: NACA0012 airfoil sample mesh. Left: whole region; right: zoomed-in figure near the airfoil.

4.7 shows a sample mesh. 30 equally spaced pressure contours are shown in Figure 4.8 and Figure 4.9. We observe that the average residual of the RKDG-MRWENO methods can reduce to about $10^{-12.5}$, near machine zero via time advancing.

Example 4.4. Two supersonic steady-state problems of NACA0012 airfoil [38] with $M_\infty = 2$, $\alpha = 1^\circ$ and $M_\infty = 3$, $\alpha = 1.5^\circ$. Figure 4.7 is also a computational mesh for this example. 30 equally spaced pressure contours are demonstrated in Figure 4.10 and Figure 4.11, respectively. It is again observed that the average residual of the RKDG-MRWENO methods can reduce to about 10^{-12} , near machine zero.

Example 4.5. Two transonic steady-state problems of NACA001035 airfoil [14] with $M_\infty = 0.8$, $\alpha = 1.25^\circ$ and $M_\infty = 0.9$, $\alpha = 0.5^\circ$. The calculation range is $[-16, 16] \times [-16, 16]$. Figure 4.12 shows a sample mesh containing 5593 triangles. Equally spaced pressure contours are demonstrated in Figure 4.13 and Figure 4.14. It is found that the residual of the RKDG-MRWENO methods can reduce to about $10^{-14.5}$, near machine zero.

Example 4.6. Two supersonic steady-state problems of NACA001035 airfoil [14] with $M_\infty = 1.5$, $\alpha = 1.5^\circ$ and $M_\infty = 2$, $\alpha = 1^\circ$. The calculation range is $[-16, 16] \times [-16, 16]$. Figure 4.12 is also a sample mesh containing 5593 triangles for this example. Equally spaced pressure contours are shown in Figure 4.15 and Figure 4.16. It is found that the average

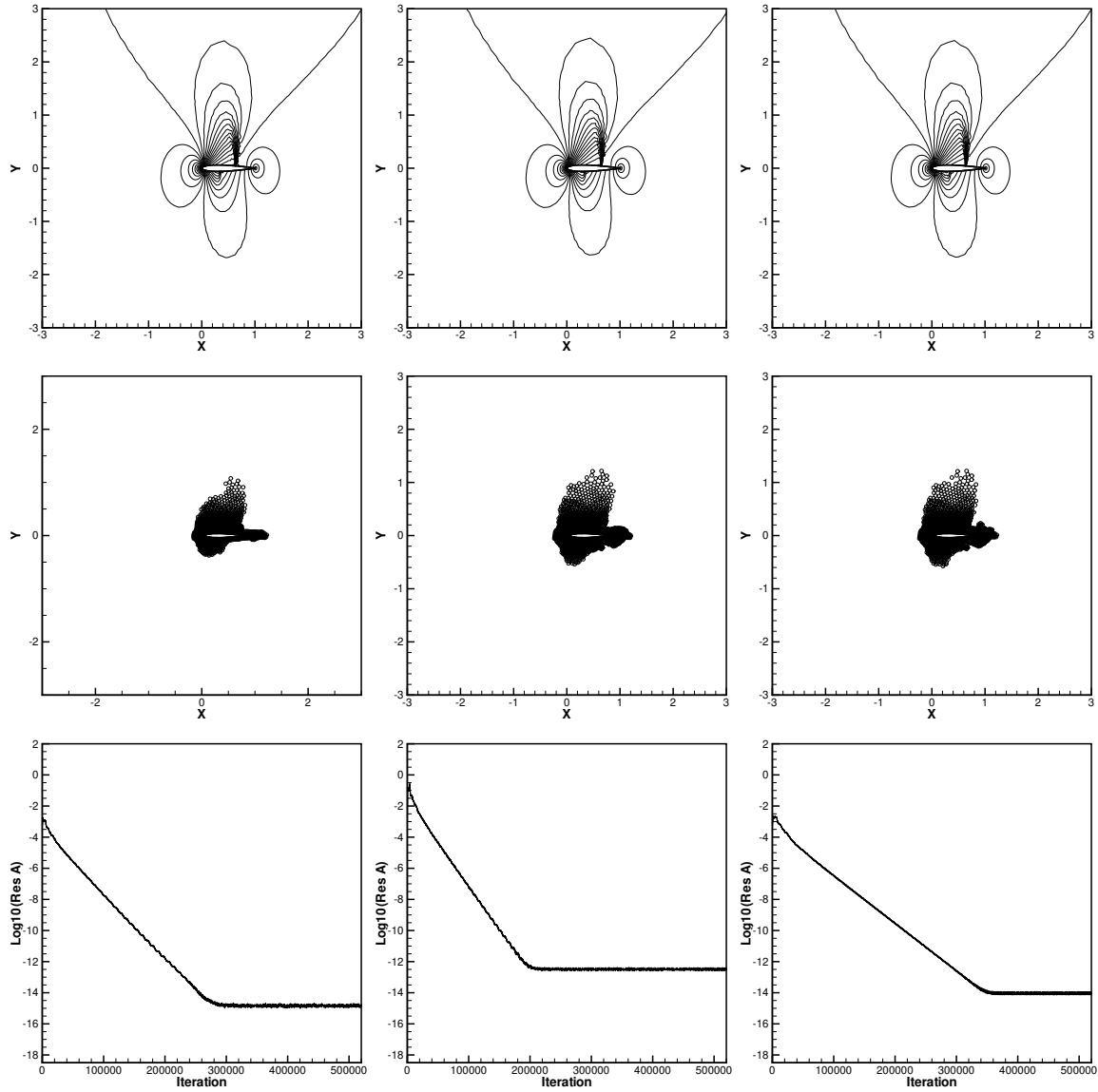


Figure 4.8: NACA0012 airfoil. $M_\infty = 0.8$ and $\alpha = 1.25^\circ$. Top: 30 equally spaced pressure contours from 0.50 to 1.46; middle: troubled cells are mainly in $[-3,3] \times [-3,3]$; bottom: the evolution of the average numerical residual. Left: RKDG2-MRWENO method; middle: RKDG3-MRWENO method; right: RKDG4-MRWENO method.

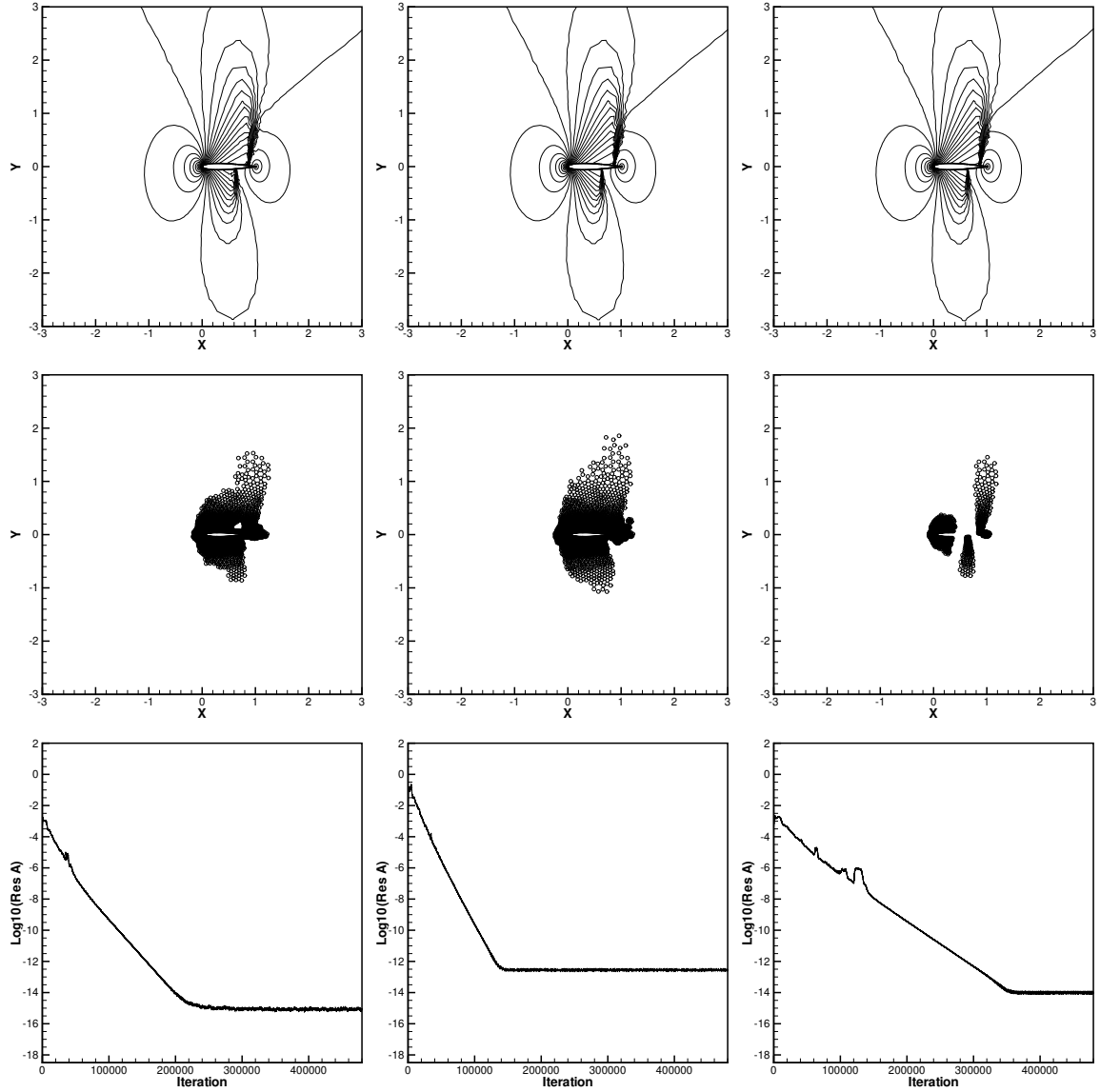


Figure 4.9: NACA0012 airfoil. $M_\infty = 0.85$ and $\alpha = 1^\circ$. Top: 30 equally spaced pressure contours from 0.49 to 1.54; middle: troubled cells are mainly in $[-3,3] \times [-3,3]$; bottom: the evolution of the average numerical residual. Left: RKDG2-MRWENO method; middle: RKDG3-MRWENO method; right: RKDG4-MRWENO method.

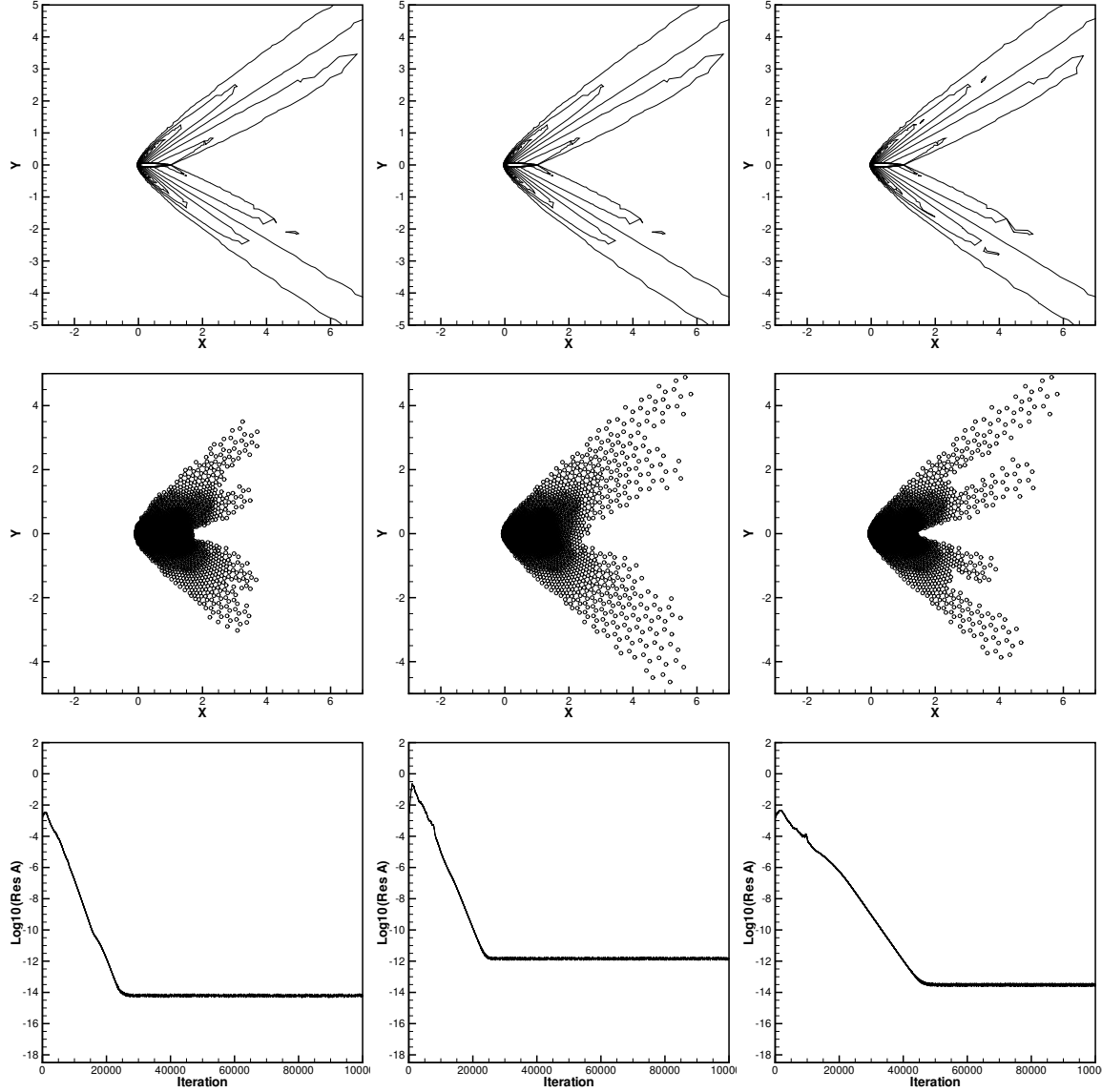


Figure 4.10: NACA0012 airfoil. $M_\infty = 2$ and $\alpha = 1^\circ$. Top: 30 equally spaced pressure contours from 0.76 to 5.35; middle: troubled cells are mainly in $[-3,7] \times [-5,5]$; bottom: the evolution of the average numerical residual. Left: RKDG2-MRWENO method; middle: RKDG3-MRWENO method; right: RKDG4-MRWENO method.

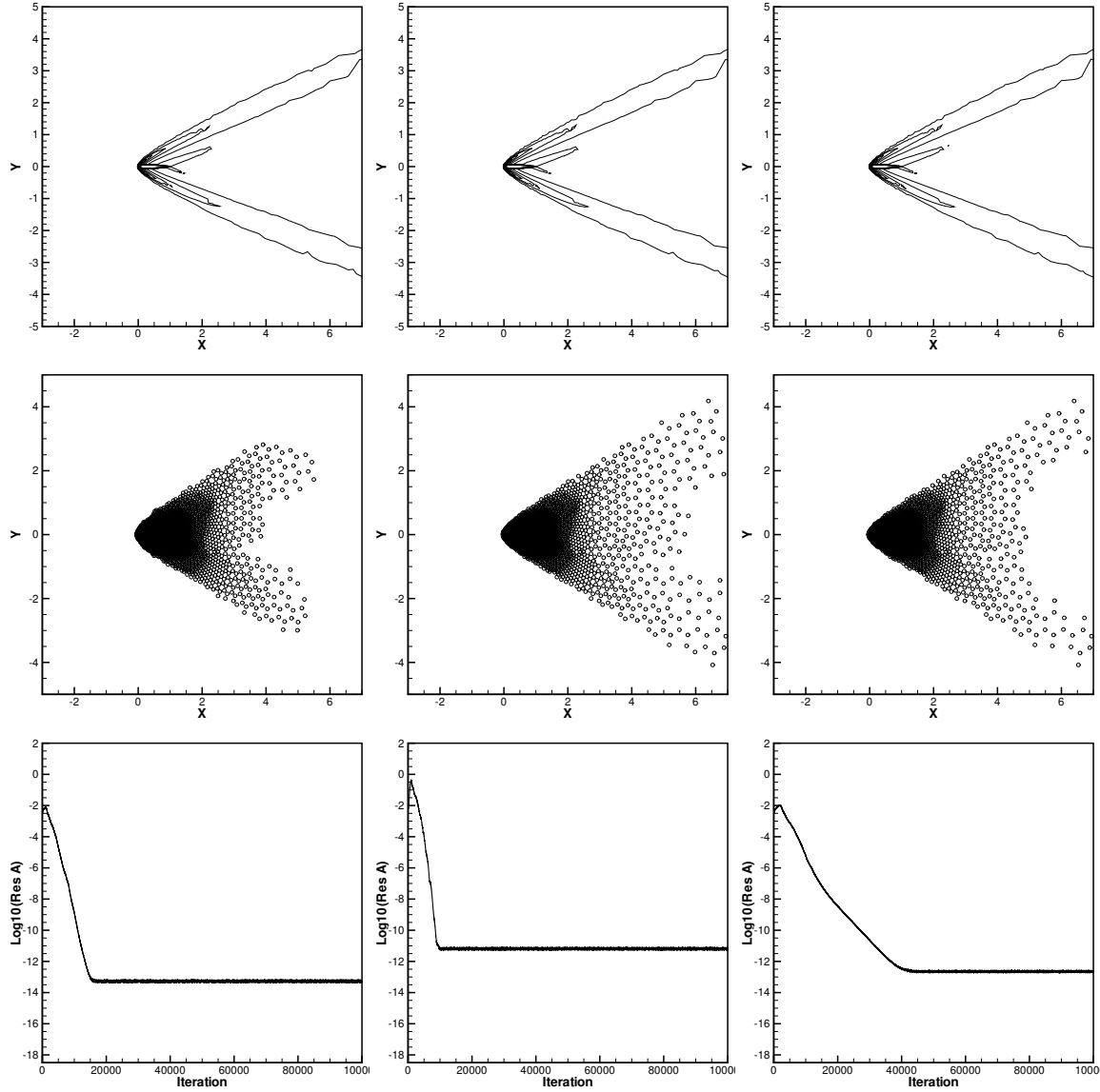


Figure 4.11: NACA0012 airfoil. $M_\infty = 3$ and $\alpha = 1.5^\circ$. Top: 30 equally spaced pressure contours from 0.76 to 11.35; middle: troubled cells are mainly in $[-3,7] \times [-5,5]$; bottom: the evolution of the average numerical residual. Left: RKDG2-MRWENO method; middle: RKDG3-MRWENO method; right: RKDG4-MRWENO method.

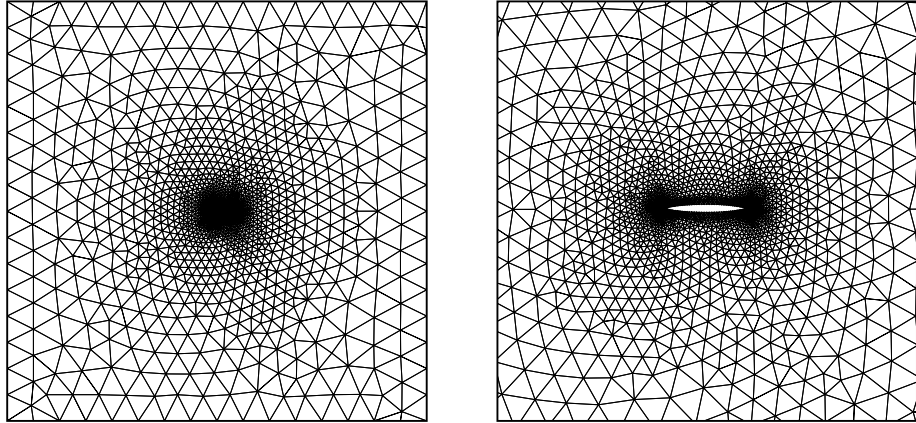


Figure 4.12: NACA001035 airfoil sample mesh. Left: whole region; right: zoomed-in figure near the airfoil.

residual of the RKDG-MRWENO methods can reduce to about 10^{-14} , near machine zero.

Example 4.7. Two transonic steady-state problems of CAST7 airfoil [14] with $M_\infty = 0.8$, $\alpha = 1.25^\circ$ and $M_\infty = 0.85$, $\alpha = 1^\circ$. The calculation range is $[-16, 16] \times [-16, 16]$. Figure 4.17 shows a sample mesh containing 5593 triangles. Equally spaced pressure contours are shown in Figure 4.18 and Figure 4.19. It is observed that the average residual of the RKDG-MRWENO methods can reduce to about $10^{-14.5}$, near machine zero once again.

Example 4.8. Two supersonic steady-state problems of CAST7 airfoil [14] with $M_\infty = 2$, $\alpha = 1^\circ$ and $M_\infty = 2$, $\alpha = 2^\circ$. The calculation range is $[-16, 16] \times [-16, 16]$. Figure 4.17 is also the sample mesh containing 5593 triangles for this example. Equally spaced pressure contours are shown in Figure 4.20 and Figure 4.21. It is observed that the average residual of the RKDG-MRWENO methods can reduce to about 10^{-14} , near machine zero once again.

5 Conclusions

In this article, a new troubled cell indicator is designed and high-order multi-resolution WENO schemes [51] are served as limiters for the RKDG methods to simulate steady-state problems on triangular meshes. The main objective is to apply the modified troubled cell

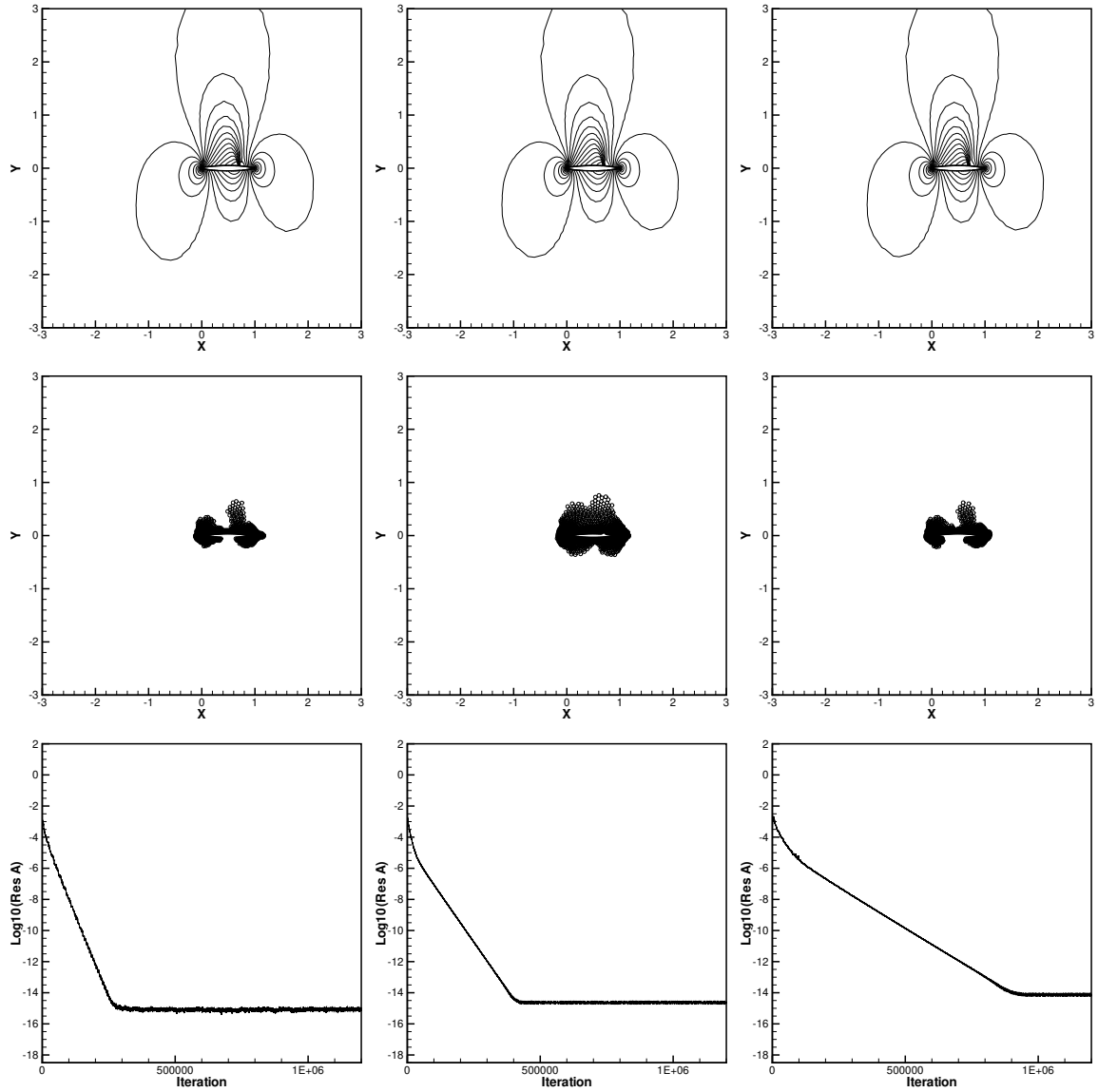


Figure 4.13: NACA001035 airfoil. $M_\infty = 0.8$ and $\alpha = 1.25^\circ$. Top: 30 equally spaced pressure contours from 0.67 to 1.43; middle: troubled cells are mainly in $[-3,3] \times [-3,3]$; bottom: the evolution of the average numerical residual. Left: RKDG2-MRWENO method; middle: RKDG3-MRWENO method; right: RKDG4-MRWENO method.

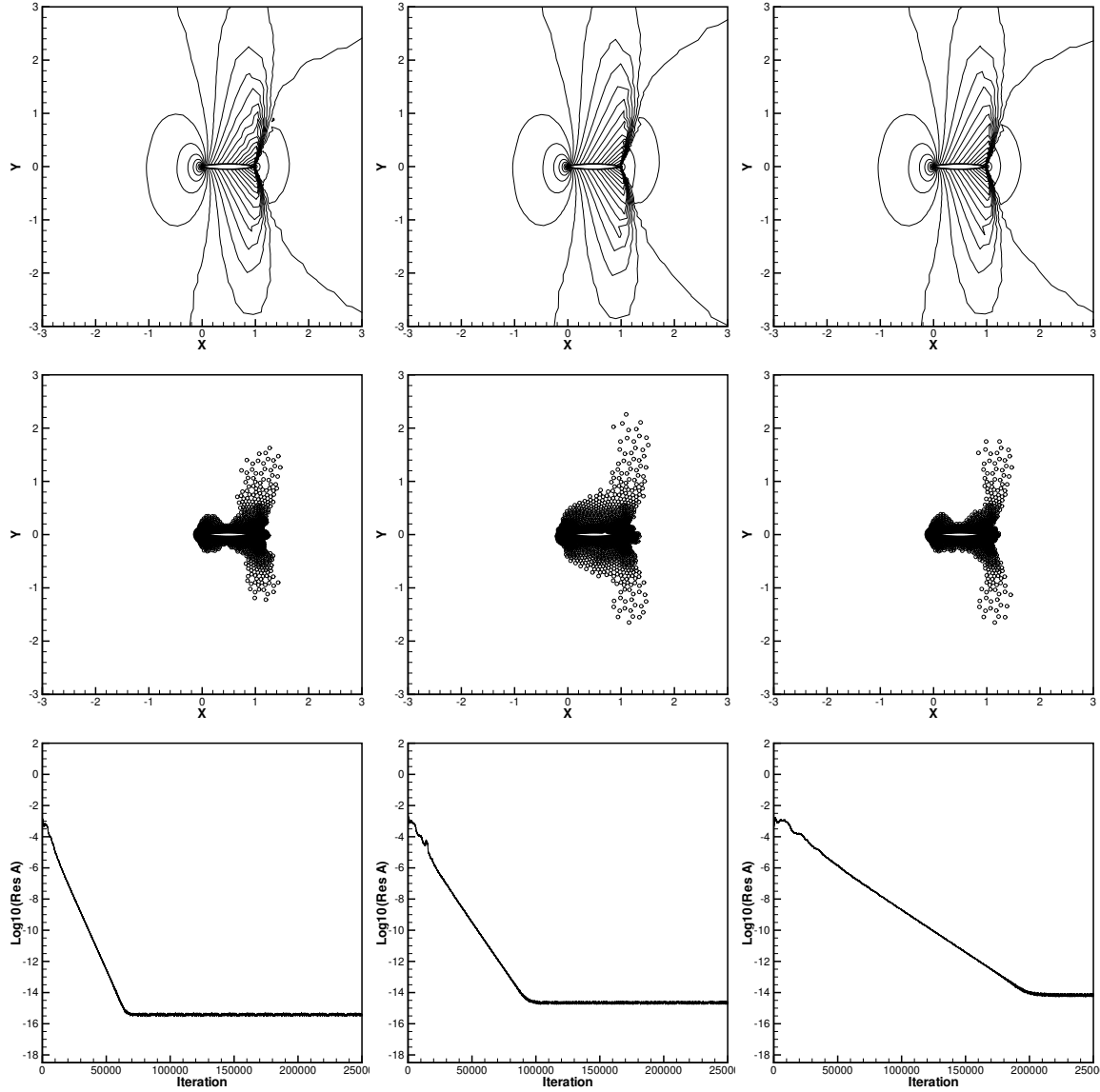


Figure 4.14: NACA001035 airfoil. $M_\infty = 0.9$ and $\alpha = 0.5^\circ$. Top: 30 equally spaced pressure contours from 0.46 to 1.58; middle: troubled cells are mainly in $[-3,3] \times [-3,3]$; bottom: the evolution of the average numerical residual. Left: RKDG2-MRWENO method; middle: RKDG3-MRWENO method; right: RKDG4-MRWENO method.

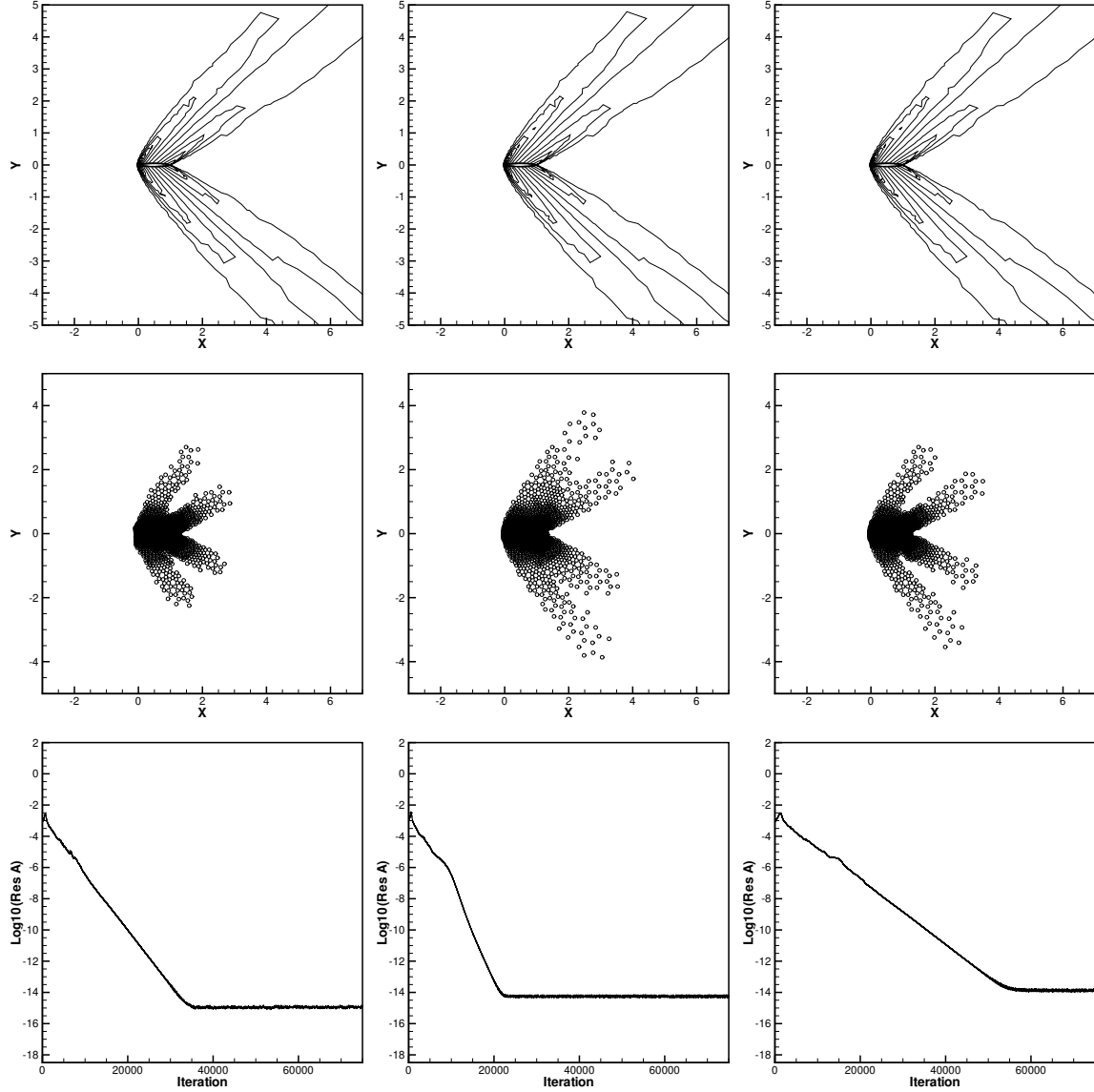


Figure 4.15: NACA001035 airfoil. $M_\infty = 1.5$ and $\alpha = 1.5^\circ$. Top: 30 equally spaced pressure contours from 0.51 to 3.21; middle: troubled cells are mainly in $[-3,7] \times [-5,5]$; bottom: the evolution of the average numerical residual. Left: RKDG2-MRWENO method; middle: RKDG3-MRWENO method; right: RKDG4-MRWENO method.

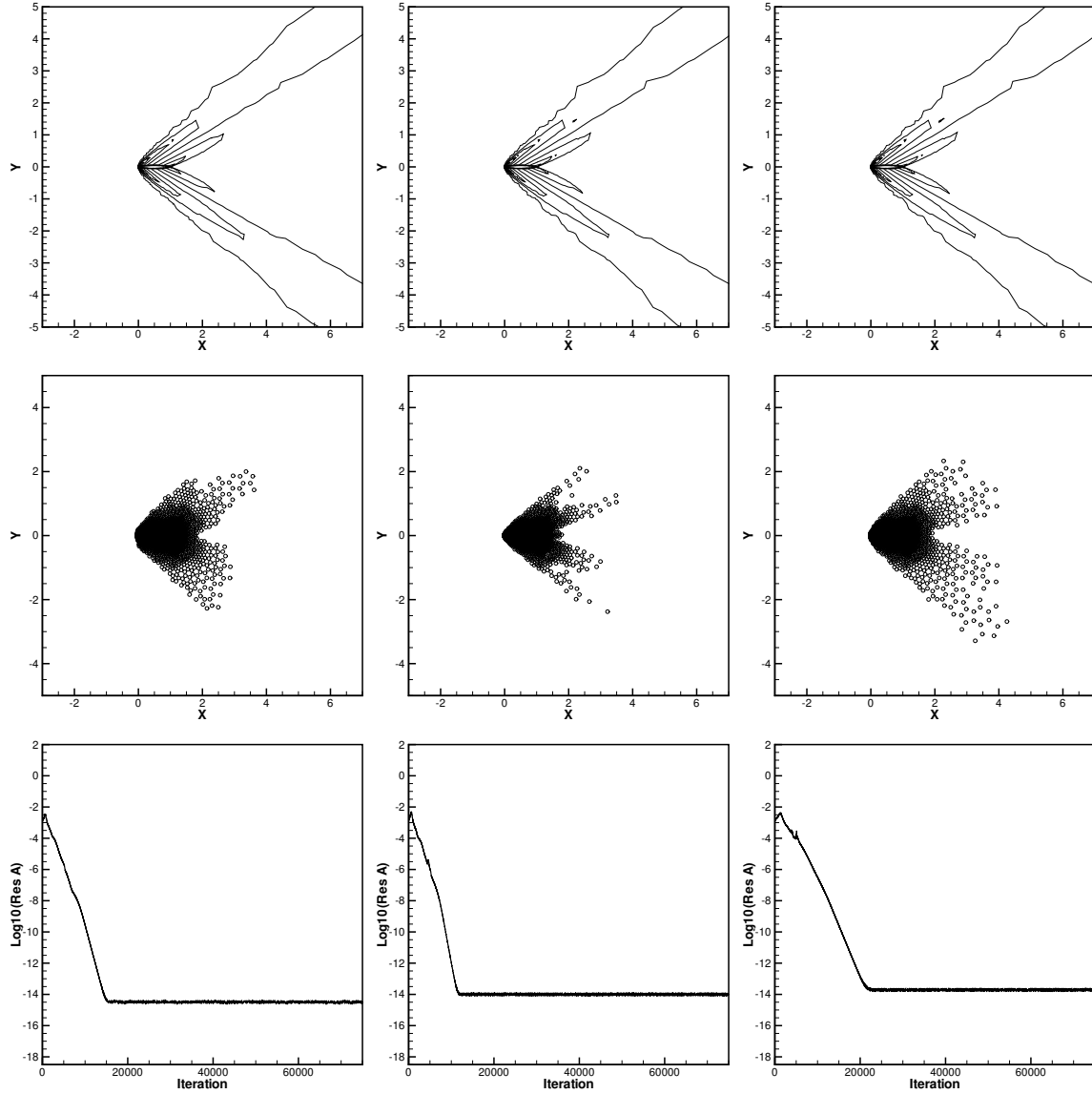


Figure 4.16: NACA001035 airfoil. $M_\infty = 2$ and $\alpha = 1^\circ$. Top: 60 equally spaced pressure contours from 0.54 to 5.15; middle: troubled cells are mainly in $[-3,7] \times [-5,5]$; bottom: the evolution of the average numerical residual. Left: RKDG2-MRWENO method; middle: RKDG3-MRWENO method; right: RKDG4-MRWENO method.

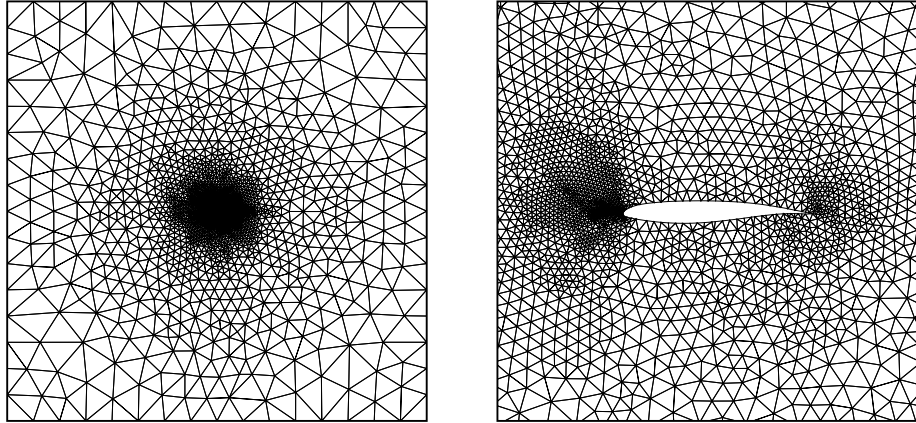


Figure 4.17: CAST7 airfoil sample mesh. Left: whole region; right: zoomed-in figure near the airfoil.

indicator to detect troubled cells subject to the multi-resolution WENO limiting procedure, and construct a sequence of hierarchical L^2 projection polynomial solutions of the DG methods over triangular troubled cell itself. By using the second-order, third-order, and fourth-order RKDG-MRWENO methods, the spurious oscillations can be well suppressed and the average residual can reduce to near machine zero. Extensive examples are applied to verify that such high-order RKDG-MRWENO methods have good effectiveness when calculating steady-state problems.

Conflict of interest statement: On behalf of all authors, the corresponding author states that there is no conflict of interest.

References

- [1] D. Balsara, C. Altmann, C. Munz and M. Dumbser, A sub-cell based indicator for troubled zones in RKDG schemes and a novel class of hybrid RKDG+HWENO schemes, *J. Comput. Phys.*, 226 (2007), 586-620.
- [2] T.J. Barth and D. Jespersen, The design and application of upwind schemes on unstructured meshes, *AIAA Paper*, 1989, 89-0366.

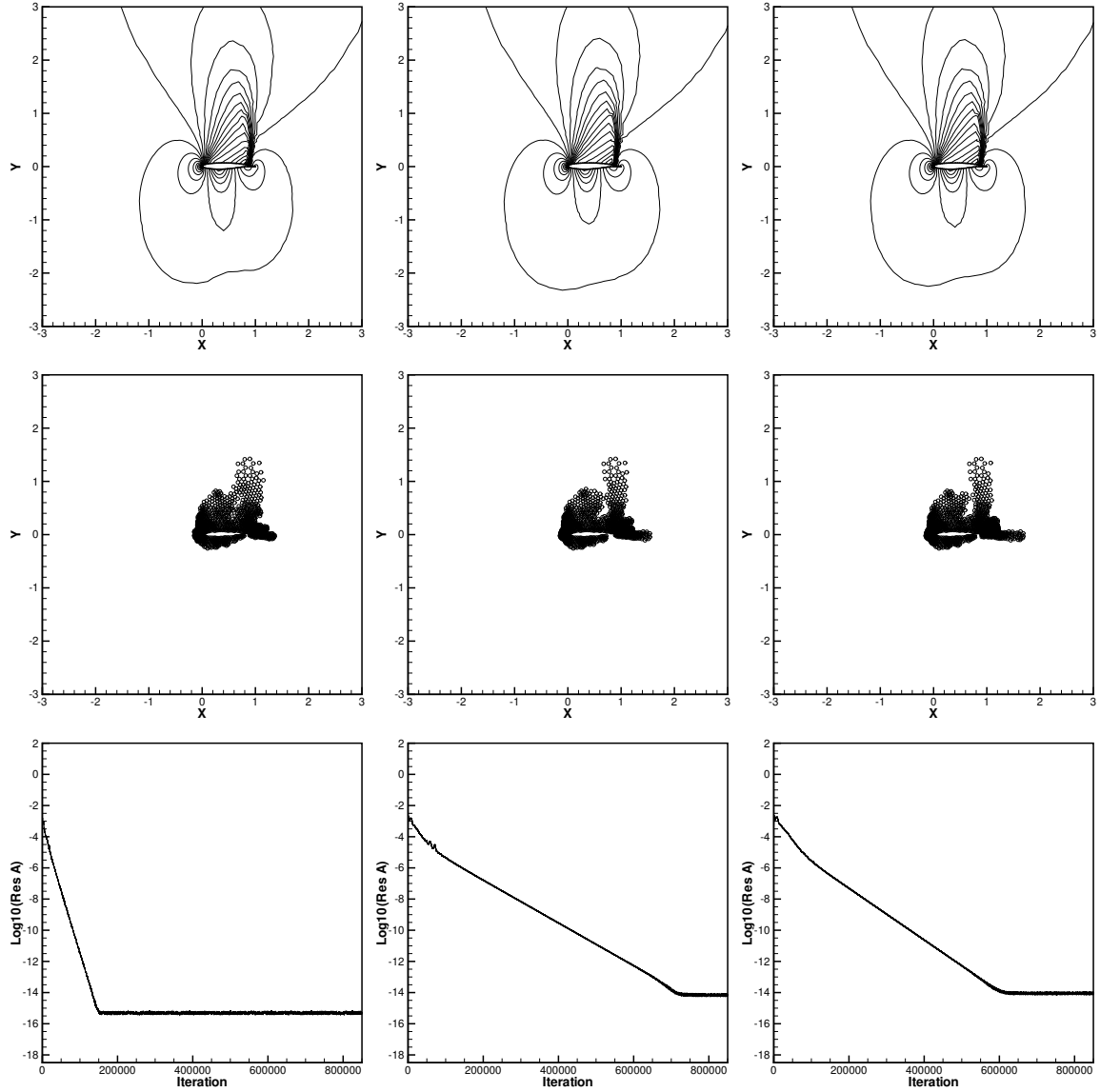


Figure 4.18: CAST7 airfoil. $M_\infty = 0.8$ and $\alpha = 1.25^\circ$. Top: 30 equally spaced pressure contours from 0.41 to 1.46; middle: troubled cells are mainly in $[-3,3] \times [-3,3]$; bottom: the evolution of the average numerical residual. Left: RKDG2-MRWENO method; middle: RKDG3-MRWENO method; right: RKDG4-MRWENO method.

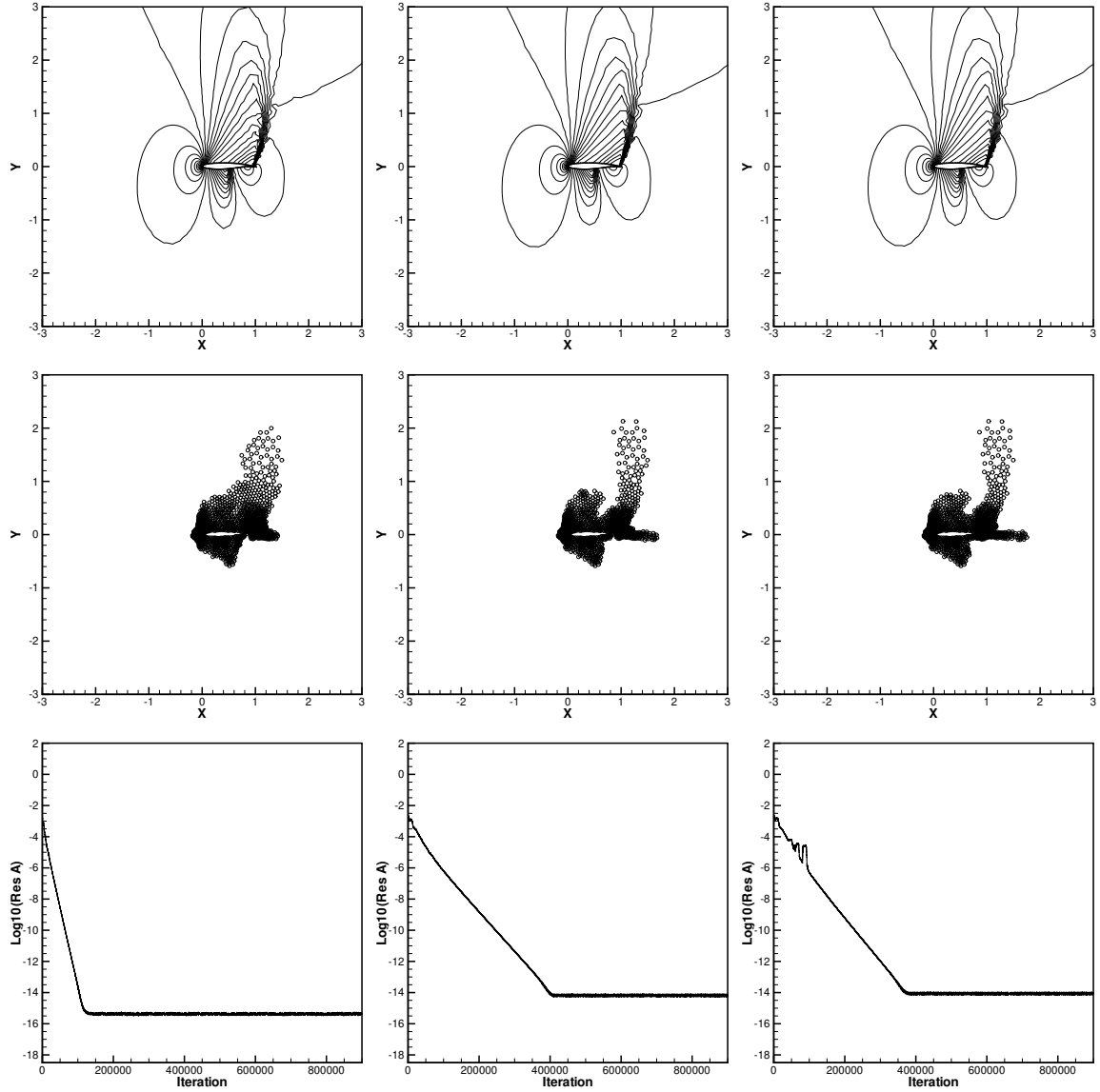


Figure 4.19: CAST7 airfoil. $M_\infty = 0.85$ and $\alpha = 1^\circ$. Top: 30 equally spaced pressure contours from 0.42 to 1.53; middle: troubled cells are mainly in $[-3,3] \times [-3,3]$; bottom: the evolution of the average numerical residual. Left: RKDG2-MRWENO method; middle: RKDG3-MRWENO method; right: RKDG4-MRWENO method.

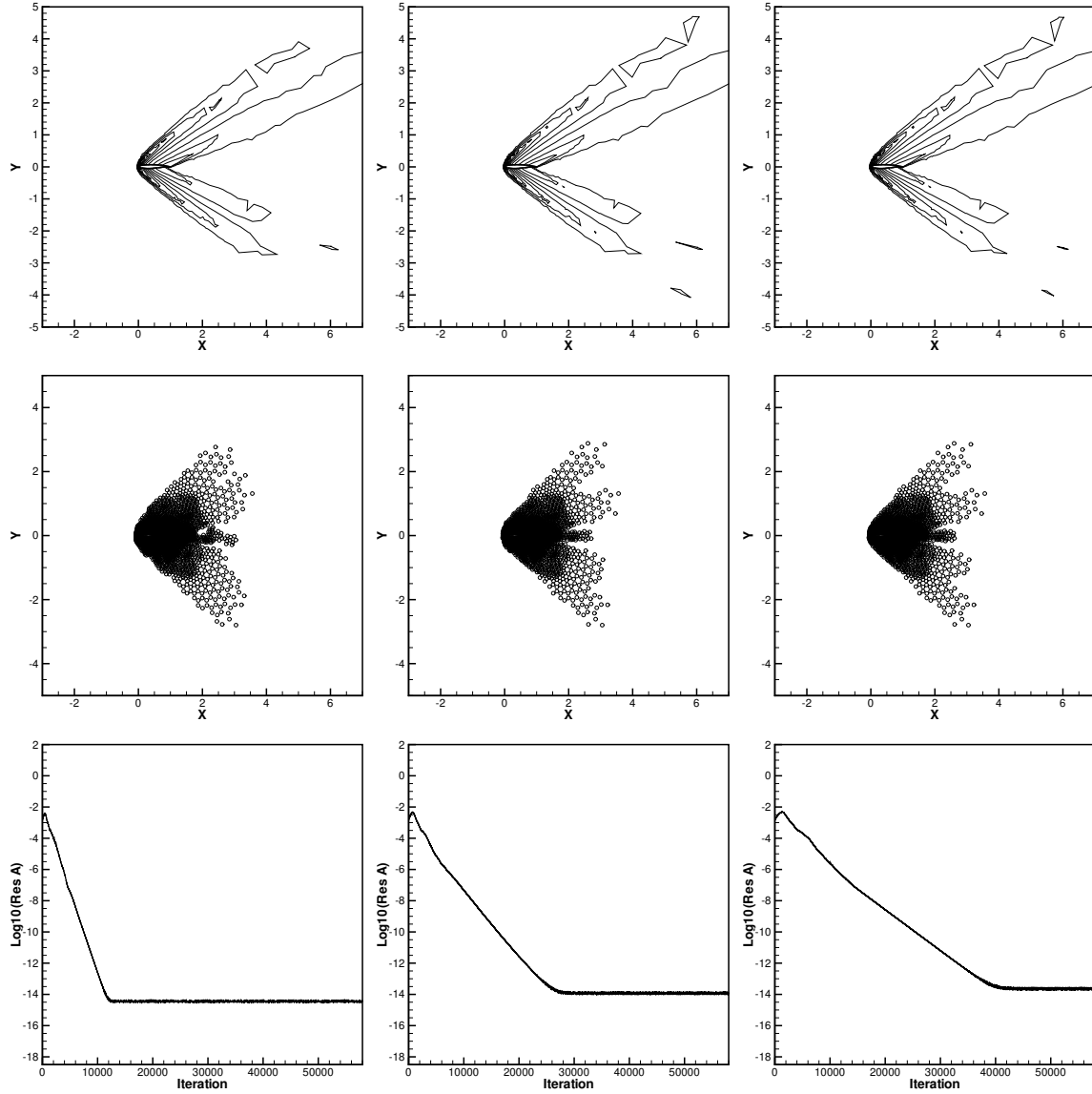


Figure 4.20: CAST7 airfoil. $M_\infty = 2$ and $\alpha = 1^\circ$. Top: 60 equally spaced pressure contours from 0.65 to 5.17; middle: troubled cells are mainly in $[-3, 7] \times [-5, 5]$; bottom: the evolution of the average numerical residual. Left: RKDG2-MRWENO method; middle: RKDG3-MRWENO method; right: RKDG4-MRWENO method.

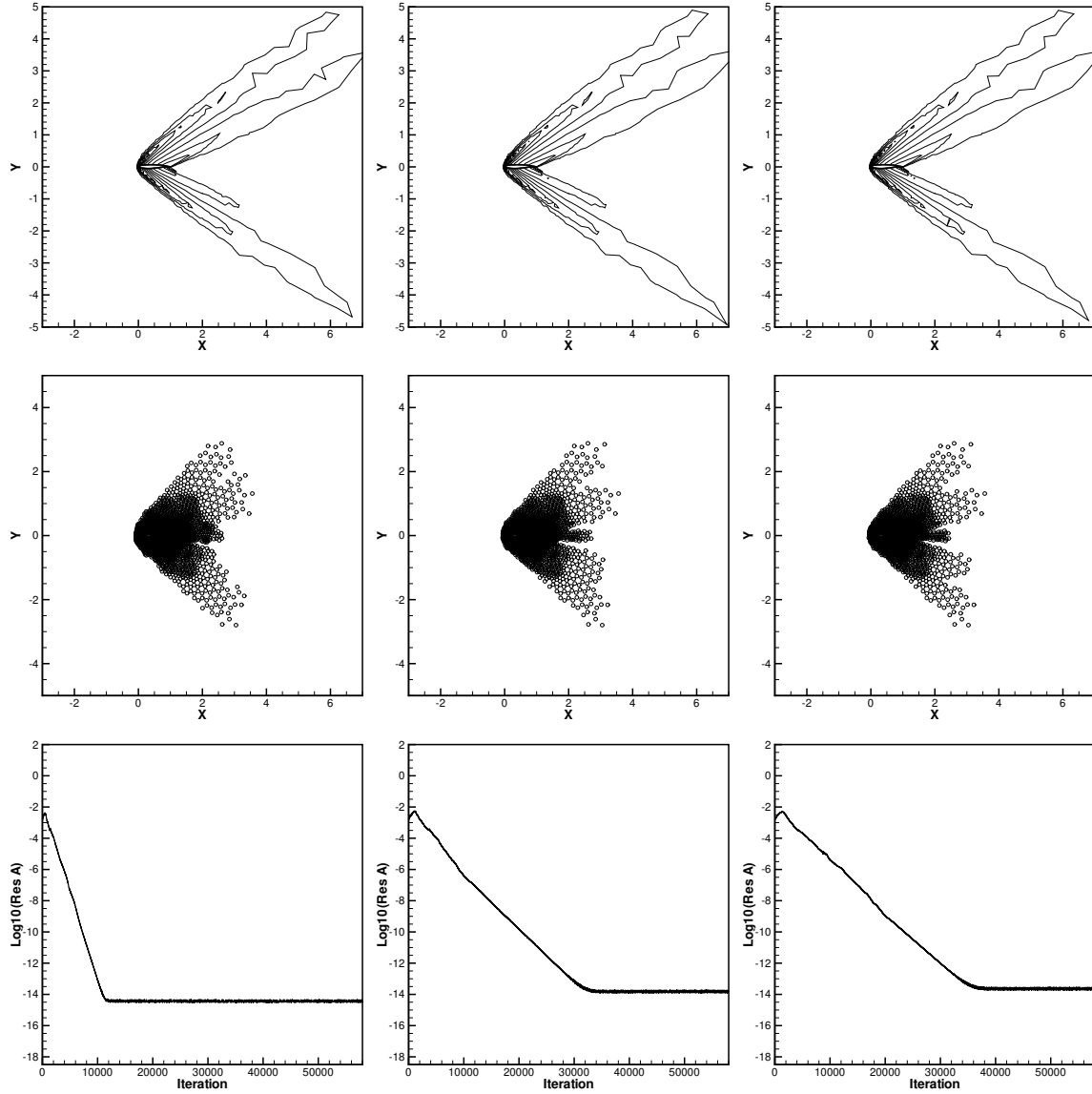


Figure 4.21: CAST7 airfoil. $M_\infty = 2$ and $\alpha = 2^\circ$. Top: 60 equally spaced pressure contours from 0.62 to 5.24; middle: troubled cells are mainly in $[-3,7] \times [-5,5]$; bottom: the evolution of the average numerical residual. Left: RKDG2-MRWENO method; middle: RKDG3-MRWENO method; right: RKDG4-MRWENO method.

- [3] R. Biswas, K.D. Devine and J. Flaherty, Parallel, adaptive finite element methods for conservation laws, *Applied Numerical Mathematics*, 14 (1994), 255-283.
- [4] R. Borges, M. Carmona, B. Costa and W.S. Don, An improved weighted essentially non-oscillatory scheme for hyperbolic conservation laws, *J. Comput. Phys.*, 227 (2008), 3191-3211.
- [5] A. Burbeau, P. Sagaut and C.H. Bruneau, A problem-independent limiter for high-order Runge-Kutta discontinuous Galerkin methods, *J. Comput. Phys.*, 169 (2001), 111-150.
- [6] G. Capdeville, A central WENO scheme for solving hyperbolic conservation laws on non-uniform meshes, *J. Comput. Phys.*, 227 (2008), 2977-3014.
- [7] M. Castro, B. Costa and W.S. Don, High order weighted essentially non-oscillatory WENO-Z schemes for hyperbolic conservation laws, *J. Comput. Phys.*, 230 (2011), 1766-1792.
- [8] B. Cockburn, S. Hou and C.-W. Shu, The Runge-Kutta local projection discontinuous Galerkin finite element method for conservation laws IV: the multidimensional case, *Mathematics of Computation*, 54 (1990), 545-581.
- [9] B. Cockburn, S.-Y. Lin and C.-W. Shu, TVB Runge-Kutta local projection discontinuous Galerkin finite element method for conservation laws III: one dimensional systems, *J. Comput. Phys.*, 84 (1989), 90-113.
- [10] B. Cockburn and C.-W. Shu, TVB Runge-Kutta local projection discontinuous Galerkin finite element method for conservation laws II: general framework, *Mathematics of Computation*, 52 (1989), 411-435.
- [11] B. Cockburn and C.-W. Shu, The Runge-Kutta local projection P1-discontinuous Galerkin finite element method for scalar conservation laws, *RAIRO Model. Math. Anal. Numer.*, 25 (1991), 337-361.

- [12] B. Cockburn and C.-W. Shu, The Runge-Kutta discontinuous Galerkin method for conservation laws V: multidimensional systems, *J. Comput. Phys.*, 141 (1998), 199-224.
- [13] B. Cockburn and C.-W. Shu, Runge-Kutta discontinuous Galerkin method for convection-dominated problems, *Journal of Scientific Computing*, 16 (2001), 173-261.
- [14] R.M. Cummings, W.H. Mason, S.A. Morton and D.R. McDaniel, Applied computational aerodynamics: A modern engineering approach, Cambridge University Press, Apr 27, 2015.
- [15] M. Dumbser, Arbitrary high order P.N.M schemes on unstructured meshes for the compressible Navier-Stokes equations, *Computers & Fluids*, 39 (2010), 60-76.
- [16] M. Dumbser, D.S. Balsara, E.F. Toro and C.D. Munz, A unified framework for the construction of one-step finite volume and discontinuous Galerkin schemes on unstructured meshes, *J. Comput. Phys.*, 227 (2008), 8209-8253.
- [17] M. Dumbser, O. Zanotti, R. Loubere and S. Diot, A posteriori subcell limiting of the discontinuous Galerkin finite element method for hyperbolic conservation laws, *J. Comput. Phys.*, 278 (2014), 47-75.
- [18] O. Friedrichs, Weighted essentially non-oscillatory schemes for the interpolation of mean values on unstructured grids, *J. Comput. Phys.*, 144 (1998), 194-212.
- [19] A. Harten, High resolution schemes for hyperbolic conservation laws, *J. Comput. Phys.*, 49 (1983), 357-393.
- [20] C. Hu and C.-W. Shu, Weighted essentially non-oscillatory schemes on triangular meshes, *J. Comput. Phys.*, 150 (1999), 97-127.
- [21] A. Jameson, Steady state solutions of the Euler equations for transonic flow by a multi-grid method, *Advances in scientific comp*, Academic Press, (1982), 37-70.

- [22] A. Jameson, Artificial diffusion, upwind biasing, limiters and their effect on accuracy and multigrid convergence in transonic and hypersonic flows, AIAA Paper, (1993), 93-3359.
- [23] A. Jameson, A perspective on computational algorithms for aerodynamic analysis and design, *Prog. Aerosp. Sci.*, 37 (2001), 197-243.
- [24] A. Jameson, W. Schmidt and E. Turkel, Numerical solution of the Euler equations by finite volume methods using Runge-Kutta time-stepping schemes, AIAA Paper, 1981-1259.
- [25] G. Jiang and C.-W. Shu, Efficient implementation of weighted ENO schemes, *J. Comput. Phys.*, 126 (1996), 202-228.
- [26] D. Levy, G. Puppo and G. Russo, Central WENO schemes for hyperbolic systems of conservation laws, *M2AN. Math. Model. Numer. Anal.*, 33 (1999), 547-571.
- [27] D. Levy, G. Puppo and G. Russo, Compact central WENO schemes for multidimensional conservation laws, *SIAM J. Sci. Comput.*, 22 (2) (2000), 656-672.
- [28] X. Liu, S. Osher and T. Chan, Weighted essentially non-oscillatory schemes, *J. Comput. Phys.*, 115 (1994), 200-212.
- [29] H. Luo, J.D. Baum and R. Lohner, A Hermite WENO-based limiter for discontinuous Galerkin method on unstructured grids, *J. Comput. Phys.*, 225 (2007), 686-713.
- [30] H. Luo, J.D. Baum and R. Lohner, A discontinuous Galerkin method based on a Taylor basis for the compressible flows on arbitrary grids, *J. Comput. Phys.*, 227 (2008), 8875-8893.
- [31] H. Luo, L. Luo, R. Nourgaliev, V.A. Mousseau and N. Dinh, A reconstructed discontinuous Galerkin method for the compressible Navier-Stokes equations on arbitrary grids, *J. Comput. Phys.*, 229 (2010), 6961-6978.

[32] H. Luo, Y. Xia, S. Li, R. Nourgaliev and C. Cai, A Hermite WENO reconstruction-based discontinuous Galerkin method for the equations on tetrahedral grids, *J. Comput. Phys.*, 231 (2012), 5489-5503.

[33] H. Luo, Y. Xia, S. Spiegel, R. Nourgaliev and Z. Jiang, A reconstructed discontinuous Galerkin method based on a hierarchical WENO reconstruction for compressible flows on tetrahedral grids, *J. Comput. Phys.*, 236 (2013), 477-492.

[34] S. Osher and C. Chakravarthy, High-resolution schemes and the entropy condition, *SIAM J. Numer. Anal.*, 21 (1984), 955-984.

[35] J. Qiu and C.-W. Shu, A comparison of troubled-cell indicators for Runge-Kutta discontinuous Galerkin methods using weighted essentially nonoscillatory limiters, *SIAM Journal on Scientific Computing*, 27 (2005), 995-1013.

[36] W.H. Reed and T.R. Hill, Triangular mesh methods for the neutron transport equation, Tech. report LA-UR-73-479, Los Alamos Scientific Laboratory, Los Alamos, NM, 1973.

[37] S. Serna and A. Marquina, Power ENO methods: a fifth-order accurate weighted power ENO method, *J. Comput. Phys.*, 194 (2004), 632-658.

[38] Y. Shida, K. Kuwahara, K. Ono and H. Takami, Computation of dynamic stall of a NACA-0012 airfoil, *AIAA journal*, 25 (1987), 408-413.

[39] C.-W. Shu, High order weighted essentially non-oscillatory schemes for convection dominated problems, *SIAM Review*, 51 (2009), 82-126.

[40] C.-W. Shu and S. Osher, Efficient implementation of essentially non-oscillatory shock capturing schemes, *J. Comput. Phys.*, 77 (1988), 439-471.

[41] C.-W. Shu and S. Osher, Efficient implementation of essentially non-oscillatory shock-capturing schemes, *J. Comput. Phys.*, 77 (1988), 439-471.

- [42] V. Venkatakrishnan, Convergence to steady state solutions of the Euler equations on unstructured grids with limiters, *J. Comput. Phys.*, 118 (1995), 120-130.
- [43] L. Wu, Y.-T. Zhang, S. Zhang and C.-W. Shu, High order fixed-point sweeping WENO methods for steady state of hyperbolic conservation laws and its convergence study, *Commun. Comput. Phys.*, 20 (2016), 835-869.
- [44] H.C. Yee and A. Harten, Implicit TVD schemes for hyperbolic conservation laws in curvilinear coordinates, *AIAA J.*, 25 (1987), 266-274.
- [45] H.C. Yee, R.F. Warming and A. Harten, Implicit total variation diminishing (TVD) schemes for steady-state calculations, *J. Comput. Phys.*, 57 (1985), 327-360.
- [46] L. Zhang, W. Liu, L. He, X. Deng and H. Zhang, A class of hybrid DG/FV methods for conservation laws I: basic formulation and one-dimensional systems, *J. Comput. Phys.*, 231 (2012), 1081-1103.
- [47] L. Zhang, W. Liu, L. He, X. Deng and H. Zhang, A class of hybrid DG/FV methods for conservation laws II: two-dimensional cases, *J. Comput. Phys.*, 231 (2012), 1104-1120.
- [48] S. Zhang, S. Jiang and C.-W. Shu, Improvement of convergence to steady state solutions of Euler equations with the WENO schemes, *J. Sci. Comput.*, 47 (2011), 216-238.
- [49] S. Zhang and C.-W. Shu, A new smoothness indicator for WENO schemes and its effect on the convergence to steady state solutions, *J. Sci. Comput.*, 31 (2007), 273-305.
- [50] J. Zhu and C.-W. Shu, A new type of multi-resolution WENO schemes with increasingly higher order of accuracy on triangular meshes, *J. Comput. Phys.*, 392 (2019), 19-33.
- [51] J. Zhu, C.-W. Shu and J. Qiu, High-order Runge-Kutta discontinuous Galerkin methods with a new type of multi-resolution WENO limiters on triangular meshes, *Applied Numer. Math.*, 153 (2020), 519-539.

- [52] J. Zhu, C.-W. Shu and J. Qiu, High-order Runge-Kutta discontinuous Galerkin methods with multi-resolution WENO limiters for solving steady-state problems, *Applied Numer. Math.*, 165 (2021), 482-499.
- [53] J. Zhu, X. Zhong, C.-W. Shu and J. Qiu, Runge-Kutta discontinuous Galerkin method with a simple and compact Hermite WENO limiter on unstructured meshes, *Communications in Computational Physics*, 21 (2017), 623-649.